

4-2018

External Cavity Diode Laser for Ultra-cold Atom Experiments

Benjamin Halkowski

Follow this and additional works at: <https://scholarworks.wm.edu/honorsthesis>



Part of the [Atomic, Molecular and Optical Physics Commons](#)

Recommended Citation

Halkowski, Benjamin, "External Cavity Diode Laser for Ultra-cold Atom Experiments" (2018).
Undergraduate Honors Theses. Paper 1221.
<https://scholarworks.wm.edu/honorsthesis/1221>

This Honors Thesis is brought to you for free and open access by the Theses, Dissertations, & Master Projects at W&M ScholarWorks. It has been accepted for inclusion in Undergraduate Honors Theses by an authorized administrator of W&M ScholarWorks. For more information, please contact scholarworks@wm.edu.

External Cavity Diode Laser for Ultra-cold Atom Experiments

A thesis submitted in partial fulfillment of the requirement
for the degree of Bachelor of Science with Honors in
Physics from the College of William and Mary in Virginia,

by

Benjamin Halkowski

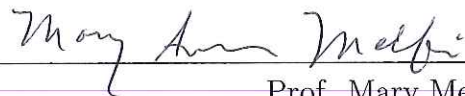
Accepted for Honors



Advisor: Prof. Seth Aubin



Prof. Timothy Costelloe



Prof. Mary Melfi



Prof. Irina Novikova

Williamsburg, Virginia
April 2018

Contents

Acknowledgments	iv
List of Figures	vi
List of Tables	vii
Abstract	v
1 Introduction	1
1.1 Project	1
1.2 The Littrow ECDL	1
1.3 Motivation	3
1.4 Structure of the Thesis	4
2 Theory	5
2.1 External Cavity Diode Laser (ECDL)	5
2.2 Free Spectral Range of the ECDL Cavity	6
2.3 Multi-mode vs. Single Mode Operation	7
2.4 Rubidium Resonance	8
2.5 Wavelength / Frequency Control	9
2.6 Doppler Broadened Absorption Line Shape	10

3	Construction	12
3.1	Initial Setup	12
3.1.1	Install Diode	12
3.1.2	Collimating the Beam	13
3.1.3	Finding Lasing Threshold	14
3.1.4	Installing Grating, External Cavity	15
3.2	Isolation	18
3.2.1	Thermal Housing	21
3.2.2	Base Buffer	21
3.2.3	Vibrational Noise from Input Wires and I/O Ports	22
3.2.4	Current Protection for Diode	23
4	Data Acquisition and Achieving Resonance	27
4.0.1	Getting Near Resonance	27
4.0.2	Aligning Fiber	28
4.0.3	Wavemeter Analysis	28
4.1	Initial Scan Range	29
4.1.1	Scan Range	29
4.1.2	Manual Scanning	31
4.2	Feed-Forward Current / Piezo Scanning Box	33
4.2.1	Feed-forward Box Construction	33
4.2.2	Voltage Regulators	34
4.2.3	Noise Reduction	36
4.2.4	Increased Scan Range	36
4.3	Temperature Drift	39
4.3.1	IR Camera	39

4.3.2	Thermistor Data Acquisition	42
5	Results and Conclusions	45
5.1	Results	45
5.2	Outlook	46
5.3	Conclusion	46

Acknowledgments

I would like to thank my research professor, Professor Seth Aubin, as well as graduate students Andrew J. Pyle, Andrew Rotunno and Shuangli Du all of whom helped me greatly while conducting my research.

I would also like to thank the ARO/VMEC grant secured by Professor Seth Aubin which helped my project in its early stages and, of course, Dr. Irina Novikova for sharing the wavemeter.

List of Figures

2.1	Simple Littrow ECDL Diagram	6
3.1	Cathode vs Anode Laser Diode Pin-outs	13
3.2	Graphic for Collimation	14
3.3	Natural Lasing Threshold Data	15
3.4	Oscilloscope: Evidence of Feedback from Grating	17
3.5	Final Configuration of Feedback	18
3.6	Initial Set Up	19
3.7	Set Up (sideview)	23
3.8	Protection Circuit Diagram	24
3.9	Set Up (overhead)	25
3.10	Set Up (external)	26
4.1	Rb Transition Levels	30
4.2	Rb Absorption Spectrum	31
4.3	Vapor Cell Resonance Emission Output	32
4.4	Feed-Forward Circuit Diagram	35
4.5	Noise in Feed-Forward Output	37
4.6	Reduced Noise in Feed-Forward Output	37
4.7	Long Scan with Feed Forward Box	40
4.8	Vapor Cell Resonance	41

4.9	Temperature Drift Evidence	42
4.10	Infrared Shot of Temperature Gradients	43
4.11	Temperature Oscillations	44

List of Tables

3.1	Temperature Table	22
4.1	Parameter Relations to Frequency	27
4.2	Table of ^{85}Rb and ^{87}Rb Transitions	30

Abstract

This thesis describes the design, construction and characterization of an external cavity diode laser (ECDL) within the context of AMO research – specifically, ultracold rubidium experiments. The main benefit over other forms of laser light is the ECDL’s low cost and narrow linewidth. Having a more narrow linewidth allows us to affect specific electron states, such as for laser cooling, more precisely than broader alternatives.

We find that building such a laser in house is feasible with scan range up to 4 GHz. We also note that attention to external noise, through mechanical vibrations but more importantly through temperature drifts, is necessary to produce an ECDL with a stable optical frequency.

Chapter 1

Introduction

1.1 Project

This thesis describes the construction and characterization of an external cavity diode laser (ECDL) for spectroscopy experiments on rubidium at 780 nm. The ECDL uses a Littrow design in which a grating reflects a fraction of the laser light back into the laser diode resulting in a narrower linewidth. The laser wavelength can be tuned via the diffraction grating angle, laser current and temperature of the laser diode over about 10 nm. Wavelengths outside this tuning window can be accessed by swapping laser diodes.

With this wavelength flexibility, we will be able to probe other substances (852 nm for Cesium-133, 718 nm for Francium-210, and possibly others) as well as other transitions of Rb and K (795 nm and 770 nm, respectively) both within the scope of Professor Aubin's research [1] and beyond [2].

1.2 The Littrow ECDL

The ECDL in this thesis uses a Littrow design which, although sensitive to vibrations and thermal drift, gives us the possibility of reaching linewidths as narrow as 100 to 500 kHz in principle and a coarse tuning range of about 10 nm. A number of

alternative designs were considered, including a Littrow design with a fixed output beam [3] and an ECDL based on an interference filter instead of a diffraction grating [4].

The Littman-Metcalf configuration, a common ECDL setup for narrow linewidths, involves the alignment of an additional mirror that reflects the light, diffracted by the diffraction grating, back into the diffraction grating and then back into the diode. This process essentially makes use of the diffraction grating twice and thus has a stronger wavelength selectivity and more narrow linewidth as a result. Also, the output beam angle does not vary as the wavelength is tuned with the mirror.

One drawback is the Littman-Metcalf's loss of zeroth order light which manifests as a significant loss in power. Also, the alignment of an additional mirror involves an increase in time spent engineering. With the Littrow supplies, and design, more or less present at the onset of our research, the choice against Littman-Metcalf was made. That being said, if narrower linewidth is required, the Littman-Metcalf would be a viable alternative after work with the current Littrow is exhausted.

In order to free ourselves from external fluctuations which can plague ECDL's with diffraction gratings, we initially thought of pursuing an alternate approach which swapped a diffraction grating for a narrow-line interference filter [4]. Instead of picking a single wavelength by the diffraction of light off the grating, the interference filter design would select wavelengths by letting a pre-specified wavelength through. We hypothesized, and were confirmed by at least one source, that this apparatus would be stable and allow us to achieve much the same results as a Littrow design [5] without worrying so much about mechanical vibrations which can jostle a diffraction grating out of position but would not affect the wavelength selection mechanics of the interference filter. The particular design of this alternative uses a cateye reflection geometry to form an external cavity centered on an interference filter. However, we

were dissuaded to follow this approach by the Thywissen research group at University of Toronto who had done work with interference filter ECDL's. This group found that they were fairly sensitive to the quality of the interference filter and they too, like the Littrow's, could not be relied upon to be shut off and turned back on without mode hopping [6].

Given that we already had the core supplies for a Littrow ECDL and the catyeye alternative did not appear significantly more promising, we chose to construct the Littrow ECDL.

1.3 Motivation

One clear possible application for the laser is as an alternate re-pumper laser. The current re-pumper laser has a linewidth of less than 15 MHz, limited by the resolution of measurement (Sinead Ryan, 2017), whereas the Littrow ECDL discussed in this thesis promises linewidths down to 100 kHz. There's reason to suspect that a narrower linewidth may offer better results by way of isolating the specific state to be re-pumped more effectively. This would be especially useful in applications such as a dark spot MOT where re-pumper laser light is sent around the ultracold atoms in an attempt to reduce thermal excitation caused by re-pumper re-emission light absorbed by neighboring particles. The effect would be a greater density of ultracold particles in the MOT.

With a broad scan range, the laser would also be ideal for probing and imaging under a wider range of conditions. More specifically, a broad scan range allows the same laser to address $5^2S_{1/2} \rightarrow 5^2P_{3/2}$ transitions that vary by several GHz, as well as when these are Zeeman-shifted by a large magnetic field.

Switching from rubidium to potassium, the Littrow ECDL offers broad sweeps in wavelength by simply replacing the removable laser diode and substituting another.

The Littrow ECDL discussed in this thesis is centered on 780 nm for rubidium. To make the laser work with potassium, one simply needs to swap the current diode for another centered around the potassium transition of 767 nm.

We could also use the laser to probe the closer 776 nm transition from $5^2P_{3/2}$ to $5^2D_{5/2}$ in both ^{87}Rb and ^{85}Rb . Alternatively, the 2-photon transition from $5S_{1/2}$ to $5D_{5/2}$ at 778 nm would also be accessible.

1.4 Structure of the Thesis

This thesis is structured in the following manner. Chapter 2 explains the theory surrounding core components of the ECDL research project. These include the main functions of the laser and the mechanics of tuning the output frequency through adjustable parameters. Chapter 3 discusses the process of constructing the laser and periphery items necessary for a fully functional ECDL. Finally, in chapter 4, we discuss results, the scan range of the laser and problems associated with temperature drifts which can cause the laser to mode-hop.

Chapter 2

Theory

2.1 External Cavity Diode Laser (ECDL)

The benefits of an external cavity diode laser lie in its narrow line-width and its tuneability. Ideally, the laser is also single mode, meaning we are outputting laser light in a very narrow range of frequencies and only those frequencies.

The Littrow configuration is based on a diffraction grating, which is used to select the wavelength by the following general relation:

$$n\lambda = d(\sin \theta + \sin \theta') \quad (2.1)$$

where n is the order of diffraction, λ is the diffracted wavelength, d is the grating constant (distance between grooves), θ is incident angle of the gain chip towards diffraction grating and θ' is exit angle of diffracted beam. For a Littrow configuration, the diffraction grating is oriented so that the first-order diffraction is reflected back into gain chip and thus $\theta = \theta'$ and thus:

$$n\lambda = 2d \sin \theta \quad (2.2)$$

which demonstrates rather succinctly the viability of the ECDL technique to scan over multiple frequencies. To change the frequency (i.e. wavelength λ), all we need

to do is change the angle of the grating θ . Figure 2.1 shows a diagram of the basic Littrow ECDL scheme.

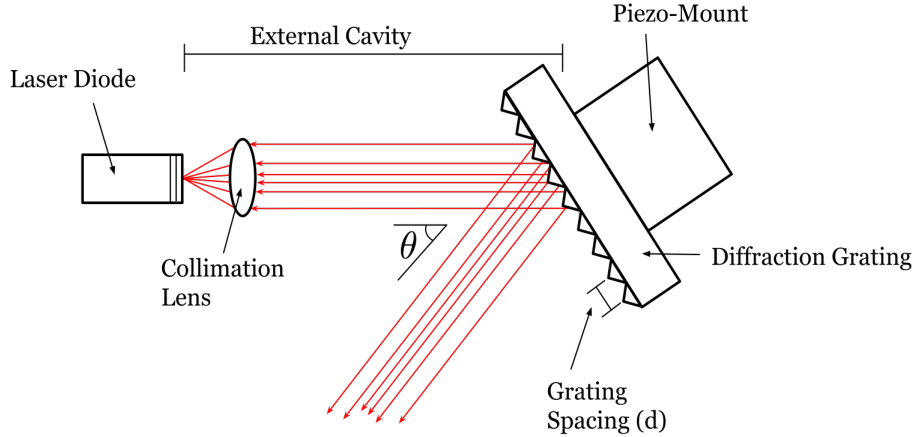


Figure 2.1: A simplistic diagram showing the core components of the Littrow ECDL design. The diode emits light at a specific wavelength according to two variables shown – the angle of diffraction θ and the grating spacing d – as well as others not shown like piezo voltage, current, and diode temperature. Both variables, from Eq. 2.2, are shown here.

2.2 Free Spectral Range of the ECDL Cavity

The external cavity, shown in Figure 2.1 has a free spectral range (FSR) of:

$$\text{FSR} = \frac{c}{2 * L} = \frac{c}{2 * 12 \times 10^{-3}\text{m}} = 12.5 \text{ GHz} \quad (2.3)$$

where c is the speed of light and L is the distance from the back of the diode cavity to the grating. This also takes into account the length of the diode itself (1 - 2 mm) multiplied by the gallium arsenide refractive index (≈ 2). That being said, the

calculation is more of an approximation, allowing us to see the general mode-hop free tuning range of the resulting laser. The FSR is the inverse of the round trip time a photon takes in the cavity of length L .

The FSR effectively limits our mode-hop free tuning which means we can expect to see a jump in mode within a 12 GHz span. Of course, mode hops may come sooner than this due to other effects which tend to change the cavity length and thus the FSR or else the gain medium conditions within the laser diode.

2.3 Multi-mode vs. Single Mode Operation

Another important aspect of a laser is whether or not the laser light is single mode or multiple mode. Multiple modes simply means that the laser is lasing at, at least, two different frequencies. Single mode means that it is lasing at a single frequency.

Furthermore, the laser may experience mode hops – abruptly changing its optical frequency – which can be seen, when viewing the rubidium vapor cell (see Figure 4.8) as a sudden drop of brightness as the frequency causing the brightness through spontaneous emission changes to another mode supported by the cavity.

For work in spectroscopy, it is necessary that the laser light is single mode as we do not want unwanted optical frequencies contaminating our experiment. The additional laser modes reduce the power of the main lasing frequency that we want and can also drive spurious atomic transitions.

This behavior is essentially a factor of the cavity and the gain medium, like all lasing processes. The cavity allows another frequency of light to be amplified with the result being multiple frequencies shown in the output.

We can check to see whether or not we have multiple modes by using a Fabry-Perot cavity. The Fabry-Perot cavity will allow the two frequencies through its cavity at slightly different points when scanning the length of the cavity through the use of

a piezo actuator. The multiple mode operation is shown as the multiple frequencies ricochet within the cavity and reach the photodiode, at the opposite end of the Fabry-Prot, at different corresponding lengths of said cavity.

We can get rid of multiple modes by making sure our beam is collimated and adjusting our ECDL output via current, temperature, cavity length and grating angle.

2.4 Rubidium Resonance

In order to be useful in the lab in our experiments with rubidium, our external cavity diode laser must be resonant with the electron energies of the element. This corresponds with having a wavelength of about 780 nm with a specific wavenumber of $12816.693 \text{ cm}^{-1}$ for the ($^{87}\text{Rb } 5\text{S}_{1/2}, F = 1$) \rightarrow ($5\text{P}_{3/2} F = 2$) re-pumper transition (see Figure 4.1).

In order to test our laser, we make use of a vapor cell which contains atoms of rubidium. When we flash our laser inside, the electrons of rubidium can absorb the photons which correspond to the energy difference between its current energy state and that of a higher level (780 nm of separation). This energy can be written as $E = \hbar\omega$, where ω is the frequency between the electron levels in rubidium multiplied by the constant 2π . The electron can occupy a number of states according to its specific quantum numbers.

After excitation, the electron can “see” an opening in a lower energy level and thus will eventually, through a process of spontaneous emission, drop down to its original energy and emit a photon with corresponding energy ($\hbar\omega$). Because this photon, in the case of rubidium, has a wavelength greater than 700 nm (i.e. 780 nm) it is in the near-infrared and difficult to observe with the naked eye. In order to see it, we must look at the vapor cell using a monochrome CCTV camera which is sensitive in the near-infrared and can detect light in this region of energy.

By shining the light through the vapor cell and using a photodiode to detect spontaneous emissions, we can see whether or not we are on resonance. The spectacle can be seen clearly with these CCTV cameras and observed quantitatively by measuring both the emission of the photons and the proportion of laser light that is absorbed by the atoms with photodiodes. For more information on observing resonance, look to Section 4.1 and Figures 4.2 and 4.1.

2.5 Wavelength / Frequency Control

The wavelength and frequency can be controlled by the adjustment of three parameters, the diffraction grating by varying the voltage sent to a piezo (thus varying the angle of the diffraction and the cavity length), the current sent to the laser diode, and the temperature of the diode.

In changing the angle of the diffraction grating, we change how the light is falling on the grooves of the diffraction grating. Specifically, we are changing the angle written in Equation 2.1, reproduced here:

$$n\lambda = d(\sin \theta + \sin \theta') \quad (2.4)$$

The angles refer to the incident and diffracted angle compared to the grating normal. When these angles are equivalent, we can simplify Equation 2.4 to $n\lambda = 2d\sin\theta$. When we adjust the piezo voltage, the piezo extends or retracts, depending on the direction, tilting the diffraction grating slightly and varying θ . The laser diode is capable of emitting many different frequencies in a broad emission spectrum and by reflecting back different portions of this broad emission into the diode, we can force the diode to start lasing on any frequency within this broad range (in this case, centered on 780 nm). Notably, our piezo which varies the angle of the diffraction grating also varies the length of the external cavity and thus the FSR.

We can also adjust the frequency by varying the current sent to the laser diode. Based on the current supplied to the diode, it will output different frequencies by changing the diode refractive index. Refraction occurs in the laser when light passes through the gain medium. By changing the refraction index, we effectively change which frequency is ultimately sent through towards the grating as output. In addition, the current can change the temperature which may change the resonance of the gain medium thus changing the overall frequency. This effect is controlled by temperature stabilization with Peltier.

As stated briefly in the other two parameters, temperature can change the output frequency by changing the frequency at which the gain medium amplifies most strongly. Effectively shifting the gain curve discussed previously. In our apparatus, we change the temperature through the Peltier Thermo-electric Cooler (TEC).

2.6 Doppler Broadened Absorption Line Shape

When directing the laser into the rubidium vapor, the atoms in said vapor will have a thermal (Maxwellian) distribution of velocities [7] meaning they will be moving. The laser frequency that resonates with these moving atoms will not be the expected 780 nm but slightly shifted in accordance with the Doppler Effect:

$$\nu = \nu_1 \left(1 + \frac{v_z}{c} \right) \quad (2.5)$$

Where ν is the new frequency for resonance for these moving atoms with velocity v_z (where z is the axis of laser propagation). The velocity distribution of the atoms is simply the Maxwellian distribution with velocity v_z . Following the derivation in [7], we simply solve Equation 2.5 for v_z and plug into the Maxwellian probability distribution P for atoms:

$$\nu = \nu_1 \left(1 + \frac{v_z}{c}\right) \Rightarrow v_z = \left(\frac{\nu - \nu_1}{\nu_1}\right) c \quad (2.6)$$

$$P(\nu_z) = e^{-Mv_z^2/2k_B T} = e^{-M\left(\left(\frac{\nu - \nu_1}{\nu_1}\right)c\right)^2/2k_B T} = P(\nu) \quad (2.7)$$

Taking note that the full width at half maximum (FWHM) of this Gaussian function is defined as the value for $\Delta\nu_{1/2} \equiv 2(\nu - \nu_1)$, $P(\nu) = \frac{1}{2}$. With this, we can solve for the new, broadened linewidth working back from Equation 2.7 which gives:

$$\Delta\nu_{1/2} = \sqrt{8k_B \ln 2} \frac{\nu_1}{c} \sqrt{\frac{T}{M}} = 2.92 \times 10^{-20} \nu_1 \sqrt{\frac{T}{M}} \text{ Hz} \quad (2.8)$$

Taking M , the mass of rubidium, to be $87 \times 1.67 \times 10^{-27} \text{ kg}$, the conditions to be room temperature ($T \approx 300 \text{ K}$) and the rest frequency to be (from the known relation $\nu = c/\lambda$) : $\nu_1 = (3 \times 10^8)/(780 \times 10^{-9}) = 3.85 \times 10^{14} \text{ Hz}$. We can calculate Equation 2.8, the broadened linewidth for ^{87}Rb at room temperature to be 513 MHz.

This is important because now we have a reference to translate peaks found during a resonance scan (see Figure 4.7) to a frequency scale. We simply measure the FWHM of the Gaussian collected as data and compare it to the known FWHM solved here. In so doing, we can find out how far our laser can scan through multiple frequencies.

Chapter 3

Construction

3.1 Initial Setup

The construction is based on previous work done on the Littrow design itself. The main components can be seen in Figure 2.1. The light from a laser diode, itself having an internal cavity necessary to produce light, is directed onto a diffraction grating which returns the first order diffraction back into the diode, thus creating an external cavity. We require steady current to power the laser diode and steady voltage to supply the piezo which controls the precise angle of the diffraction grating.

All optical components are secured to an optical base plate by the use of forks which make sure our system remains rigid. Rubber isolation shields this top optical breadboard from the main optical table (see Figure 3.7).

3.1.1 Install Diode

The diode we use in the working laser is a Sanyo DL-7140-201. To wire the diode correctly to the current supply, it was important to research whether or not the diode was cathode grounded or anode grounded. This is simply a question of polarity. Do flowing electrons travel from the anode to cathode, or cathode to anode? As it turns out, the Sanyo diode, produced by SANYO Electric Co., Ltd. Semiconductor Business Headquarters, is a cathode grounded laser corresponding with the pin-out

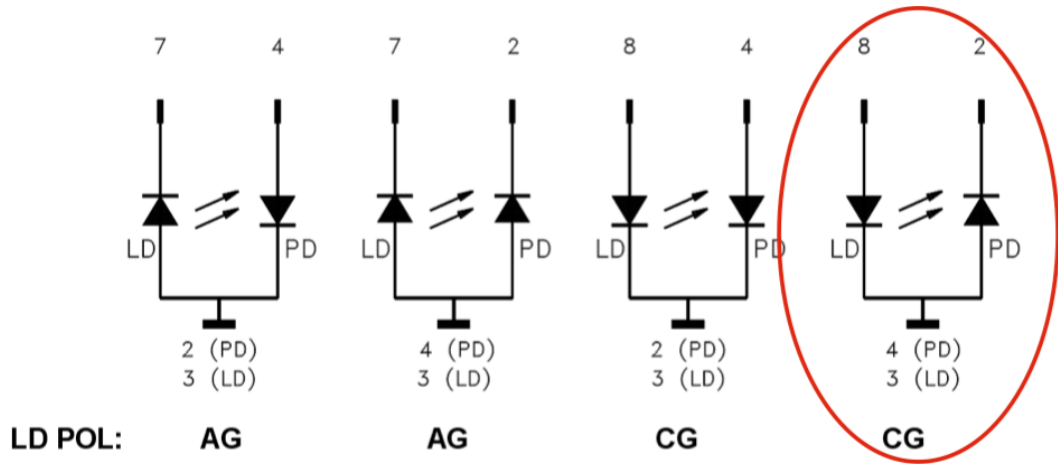


Figure 3.1: Taken from the THORLABS product specifications for the LDC202C, we see the current Sanyo laser diode with its configuration circled in red. This is the configuration necessary for the wiring into the current supply.

shown in Figure 3.1.

Knowing the polarity, we know the correct way in which to connect the input current to the diode. For vibration isolation, we make sure to use ‘floppy’ wires which are very thin and poor conductors of mechanical vibration, to connect the laser diode with the pins on the THORLABS LCD202C current supply.

3.1.2 Collimating the Beam

The next step after installing the diode is to collimate the output beam. We use a collimation tube in which the collimation of the output beam is set by the distance between the lens on the end of the tube and the laser diode. The lens is convex, and it takes a diverging beam and attempts to constrain the resulting light cone. Too far away, and the beam becomes converging, too close and the beam still diverges. The collimated beam should consist of parallel rays and be as unchanging as possible as it travels away from the lens. The different modes of collimating can be seen in Figure 3.2.

The collimation exercise involves getting the laser diode to emit light and then

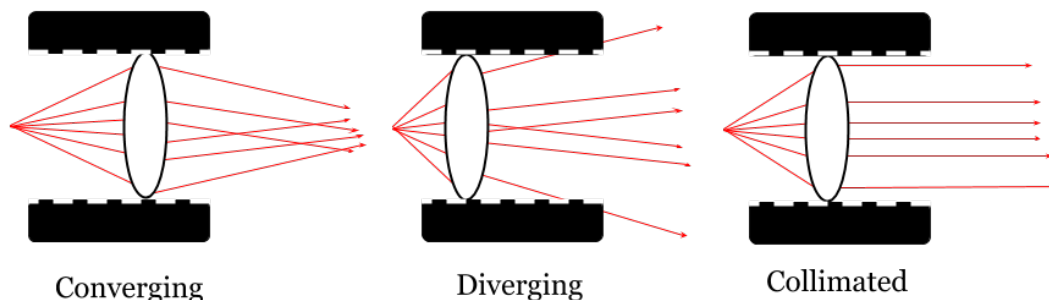


Figure 3.2: We can see the different stages one reaches while collimating the lens. The lens shown above is moved left and right through the tube by screwing the lens in and out. Irregularities in the lens meant that screwing not only changed the distance which is the desired change, but also the angle of incidence for the laser light, which is not desired. The result made collimation rather more time consuming than one might hope.

create a path long enough to see the converging or diverging of the beam. This path creation was made with a number of mirrors which reflected the beam in a relatively confined space, thus maximizing path length and any effects of converging or diverging. It was extremely important to check the entire path as converging and diverging spots could sometimes be visible in parts of the path but not in others.

3.1.3 Finding Lasing Threshold

After collimating with the lens, we want to know what our natural lasing threshold is without any feedback from a grating. This is equivalent to finding the lasing threshold without an external cavity. The method is to place a power meter in front of the beam emitted from the diode/collimation tube and vary the current for the diode until we see a steep increase in power output. The resulting output can be seen in Figure 3.3.

From the threshold line fit in Figure 3.3, we can find the moment of lasing as its intersection with the linear ground level:

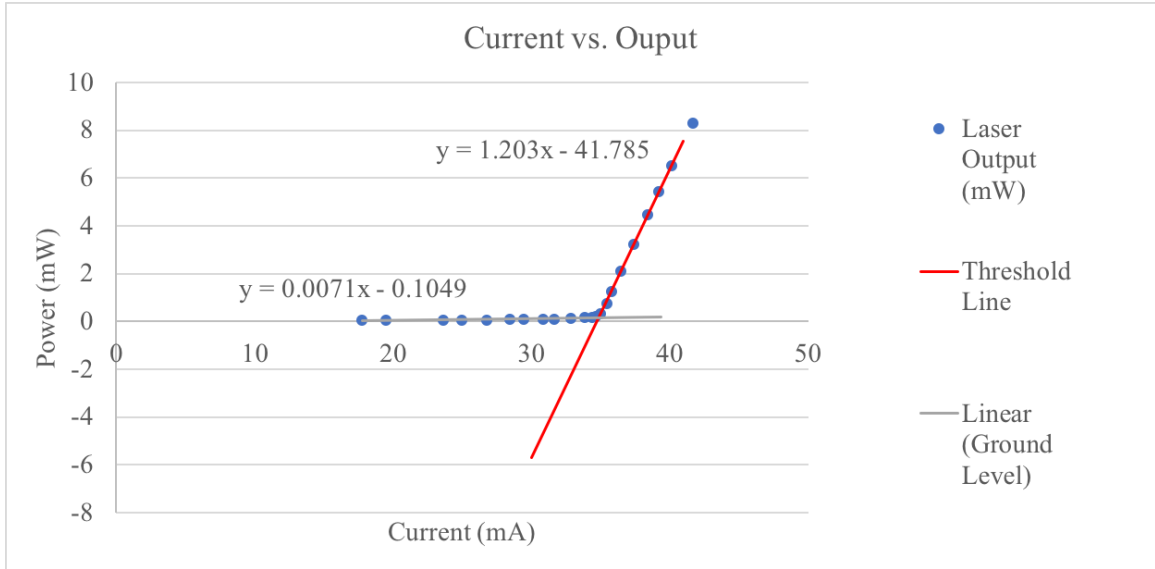


Figure 3.3: Natural lasing threshold plot obtained from power meter and laser diode collimation tube set up.

$$0.0071x - 0.1049 = 1.203x - 41.785 \quad (3.1)$$

$$x = 34.85\text{mA} \quad (3.2)$$

Above this level of current, and the laser begins the stimulated emission process resulting in an output beam.

3.1.4 Installing Grating, External Cavity

The next step is to install the grating into the setup. We can see the initial implementation in Figure 3.6 before vibration isolation was implemented. In the final set up, we see that although the apparatus has changed significantly with additional noise isolation, the setup with grating and laser diode in Figure 3.7 still bears resemblance to both the earlier setup and the simplified diagram of a Littrow ECDL (see Figure 2.1).

The grating is used to select the frequency and narrow the linewidth. We secure

the collimation tube to a pedestal affixed atop a Peltier TEC controlled by the temperature controller (Temp. Controller WTC3293-14000 Series) and affix grating to a similar pedestal in the path of said laser diode configuration. At an early stage it is important to construct a setup that will be thermally isolated. We will look more into this aspect in the following section on isolation.

We want the first order diffraction to bounce directly back into the diode from the grating. This should occur at roughly a 45 degree angle. While placing the grating pedestal in front of the secured diode pedestal, we keep track of where the first order deflection is going (this coarse adjustment is tuned with the screws on the grating).

We found that it works best if you can get the grating first order reflection to show up on the rim of the collimation tube (to the right or left of center reflection). This way you know which way to adjust.

At this point, we connect a photodiode and function generator to an oscilloscope. The function generator is connected to the laser current supply and sends a triangle wave to scan the current forward and back across the lasing threshold which was found previously with power meter (around 35 mA). (It is important that we not send negative voltage to the diode. Doing so can cause catastrophic damage to the electronics inside and is in fact the motivation behind a dedicated protection circuit discussed later). The photodiode will read the resulting zeroth order reflection from grating.

We tune the grating with screws that adjust both x and y axis tilt. In this way, we can send light from diode straight back from grating. When this is achieved we start to see the resulting behavior on the oscilloscope measuring the photodiode response. The scanned power appears as a triangle wave – with small wavy hills and valleys. We see in Figure 3.4 that achieving feedback with a grating greatly reduces lasing threshold meaning we can lase without sending as much current. This reduction

means we can achieve more lasing power at a given current.

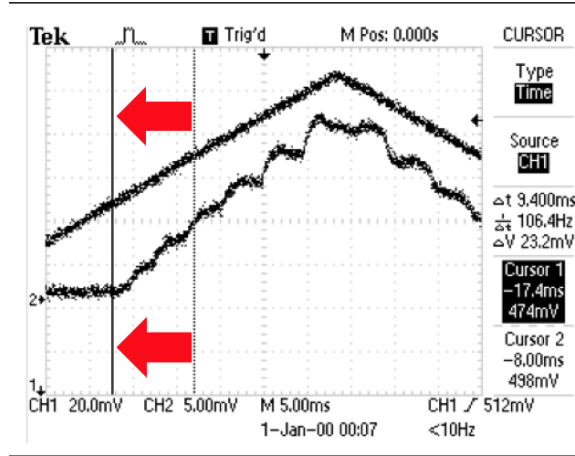


Figure 3.4: We see in the oscilloscope both the oscillating signal being sent to the current driving the laser diode and the resulting output from the photodiode. The wavy pattern is a sign of reflection from the grating. The lasing threshold, the increase of the signal from flat to peak, is moved to a lower current thanks to said feedback. The feedback here is only partial. The next figure shows the more pronounced final feedback configuration. (Figure 3.5)

We found during setup that it is far easier to achieve feedback when the grating is far away from the diode. This is because the range of angles that will give any sort of feedback is much narrower than the range when the grating is very close. Furthermore, the one angle that gives feedback is much more likely to be the most effective feedback when the grating is further away simply based on the angle the reflection has back into the diode. The method was to achieve this max feedback further out and try to maintain the angle while moving the grating further into the diode. In practice, we can only maintain the vertical angle direction while the horizontal angle needs to be adjusted in the grating's new location, closer to the diode (see Figure 3.9).

Lasing Threshold, Percent Reduction

Working from the data in Fig. 3.5, we can achieve the following percent reduction.

We calculate the percent reduction by first solving for the current based on voltage

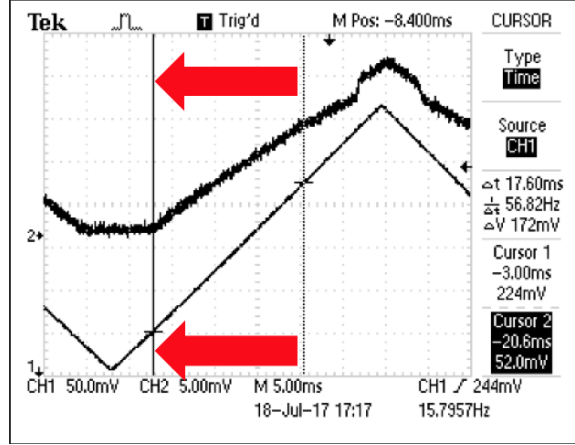


Figure 3.5: Shown here is the final configuration for feedback. Notice that the lasing threshold is pushed back severely. The dotted line once again shows where the signal initially jumped (laser started lasing) and the solid line shows where the laser is now lasing. Recall that we are showing the photodiode output (fuzzy line, CH 2) with laser power (CH 1).

sent into current:

$$I_{LD}(mA) = I_{LDSet}(mA) + I_{LDMAX}(mA) \frac{U_{mod}(V)}{10(V)} \quad (3.3)$$

$$I_{LD}(mA) = 30.55(mA) + 200(mA) \frac{.052(V)}{10(V)} = 31.59mA \quad (3.4)$$

Knowing the final current needed to lase with the help of feedback (31.59 mA) and knowing the current needed to initially lase without feedback (34.85 mA), we can calculate a percent reduction based on our feedback configuration:

$$\text{Percent Reduction} = \frac{34.85mA - 31.59mA}{34.85mA} = 9.35\% \quad (3.5)$$

3.2 Isolation

The biggest problem in a Littrow design or any diffraction grating ECDL is the sensitivity to external fluctuations. Of course these external fluctuations are but one

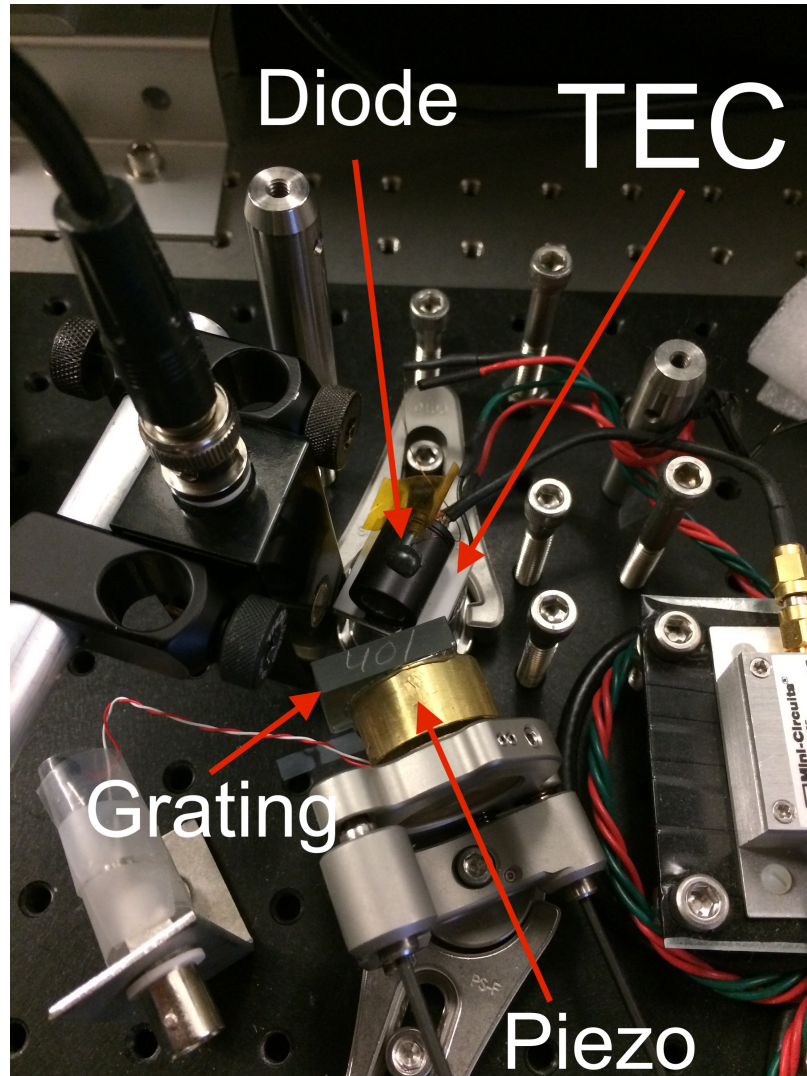


Figure 3.6: We can see here some of the main components at work in our initial coarse set up without any isolation. The TEC is the Peltier attached to the temperature control, the piezo adjusts the diffraction grating's angle, also shown. The diode is our source of laser light contained in our external cavity design.

source of frequency changes. Another is the purely theoretical source of the cavity which can offer disturbance for particular mode operation through mode-hopping.

External fluctuations can cause mode hops which can cause unpredictable and undesirable changes in output frequency. In order to be of most use, the ECDL should predictably output a given frequency at least well enough to be laser locked.

In an ideal world, we would have perfect isolation and enjoy perfect resonance with single mode and very narrow linewidth. But in the real world, we do our best to reduce noise as much as possible and produce the cleanest signal.

We start by noticing a strong correlation between changing the temperature via the TEC and the laser output frequency. Thus, we conclude that temperature has a strong dependence on output frequency and should be isolated as much as possible. Hence, the first order of business is to create a housing to prevent any draft in the room from changing the temperature of the diode/cavity and thus changing the resonant mode.

Another source of external noise comes from mechanical vibration. Vibration caused by knocking a part of the apparatus, or fiddling with wires, will cause vibrations to run throughout our system. These vibrations could cause a mode hop by ever so slightly jostling the internals of our ECDL. For this reason, it is in our best interest to create a buffer between the base in which the optical elements sit and the table in which we have a number of other things which could cause vibrations (an obvious culprit is the upper shelf added on top of the optics workstation). Vibration isolation was achieved with a layer of sorbothane and an additional piece of aluminum (see Figure 3.7). Having more than one material helps to reduce vibrations.

3.2.1 Thermal Housing

At first, robustness was our main concern and thus we constructed a housing made out of aluminum complete with I/O ports and a hole in place for the output beam. The resulting house was sturdy but left room for improvement in one respect. In our initial adjustments, access to the grating mount was necessary: this meant that the cover would need to be off. Then, once set, the housing must be replaced to provide thermal isolation. The problem arises in the replacement of the housing as the securing method used to fix the ECDL to the optics table did not allow access to screw holes meant to fix the housing back on the ECDL. Adjustments to the grating must be made after the laser is placed on the optics table and that requires access to the grating itself. Possibilities of implementing some type of funnel to get to the screw even with a housing intact were considered but ultimately abandoned and a simpler and equally effective solution was implemented.

For this, we simply use cardboard which is cut precisely to sit on the optics table fully covering the laser system (see Figure 3.10). A hole is then added for the laser output beam. This design has the benefit of easy removal and replacement, necessary conditions for the alignment process. It also greatly reduces frequency swings due to air currents within the lab affecting the temperature, and thus the length of the cavity.

3.2.2 Base Buffer

We started out trying to achieve stable resonance with the Thorlabs aluminum optical breadboard flush with the main optic table. That is, the black board in Figure 3.7 lying on the table without the layers of vibration protection. Simple vibrational tests — causing vibrations intentionally and observing the effects on the laser output — confirmed that vibrations from the surrounding setup could lead to output instability.

As a solution, we placed layers of sorbothane and a layer of aluminum to deaden the vibrational noise from elsewhere in the setup (see Figure 3.7). Although initially concerned that the optical breadboard, once separated from the large optic table, would not be a sufficient heat sink for the heat producing diode and, more importantly, the TEC, this turned out not to be an issue. Using a thermistor, we measured temperatures on different parts of the optical breadboard to check for possible thermal length fluctuations but found minimal temperature change with varying position.

Table 3.1: Optical table temperatures — test for thermal induced length change before Base Buffer

	Far side of diode $\pm 0.1^\circ\text{C}$	Near diode $\pm 0.1^\circ\text{C}$
Optic Table	21.2°C	21.3° C
Base Plate	22.0°C	22.3° C

The minimal temperature change’s effect is further reduced by leaving the apparatus running as any change in cavity length would cease once the temperature had gained stability. However, it turns out the existing TEC does not reach stability but instead oscillates somewhat, causing frequency shifts (Section 4.3.2).

3.2.3 Vibrational Noise from Input Wires and I/O Ports

In part of our initial build, the I/O panel (see in Figure 3.9) was built separate from the aluminum housing. The idea was to decrease any small vibrational impact plugging cables in and out would have on the apparatus.

Noise reduction was further realized by installing an intermediary connection between the I/O ports and the plugs to our TEC and current supply. The intermediary connection is made with very thin, flexible wires in an attempt to decrease disturbances caused by heavy cables weighing on the system.

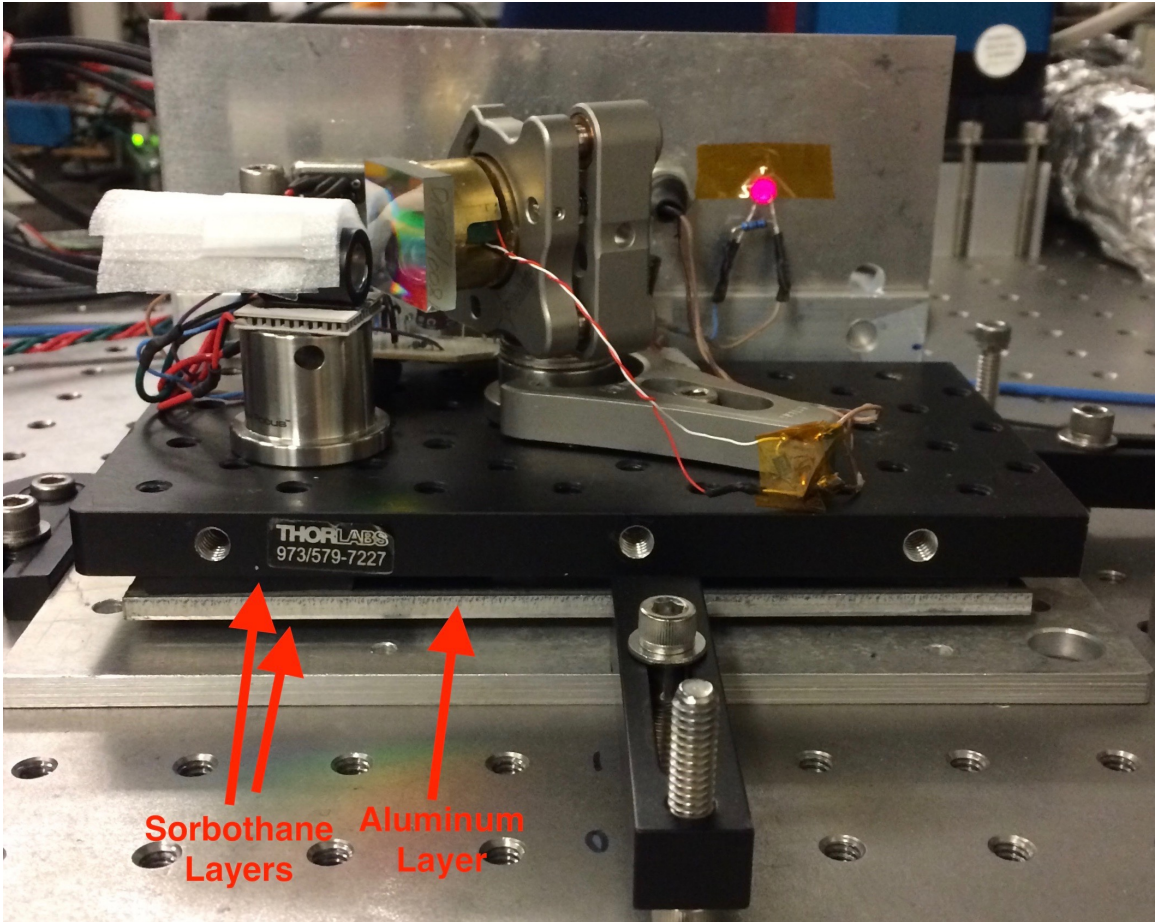


Figure 3.7: Here we can see the additional layers which will reduce vibrations which threaten to mode hop our laser and get it off resonance. Note that the housing has been removed for this photograph.

Furthermore, our base vibration buffer, described rigorously in the previous section, further reduced possible mechanical vibration from the I/O port by putting the optic platform, on which the laser sits, above the I/O port's connection to the lower aluminum slab. In this way, the possibility of direct vibrational impact on the apparatus by the I/O ports is dramatically reduced.

3.2.4 Current Protection for Diode

After aligning the laser and fitting additional noise reduction devices to the system (necessary in our attempts to reduce the possibility of mode hopping by the laser), we

still have the issue of effectively powering the laser itself. We employ the LCD202C current supply from THORLABS to provide low noise current for our Sanyo DL-7140-201 laser diode. However, we still wanted to make sure that the laser will be safe from unintentional input in the form of a reverse flow of current, for example, if the input voltage ports were somehow reversed, and we put negative to positive and vice versa.

The solution was to implement a current protection circuit the result of which can be seen in Figure 3.9. The circuit was constructed with a number of capacitors of differing capacitances arranged in parallel to deal with any negative voltage coming across (see circuit diagram in Figure 3.8). The working board can be seen in Figure 3.9.

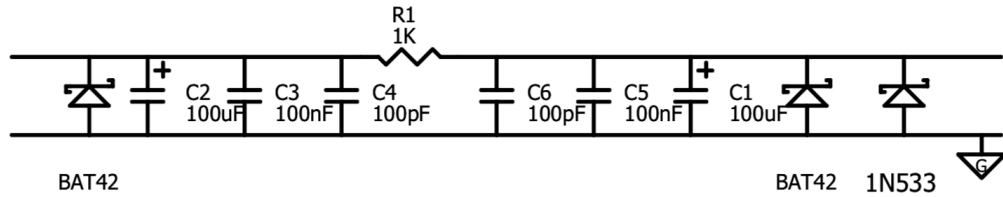


Figure 3.8: Here we use a series of capacitors to make sure that any negative voltage put across the terminals is swallowed by the diodes. Also, high frequency noise is mitigated by the series of various capacitors, each, in turn reducing a separate range of possible high frequency noise.

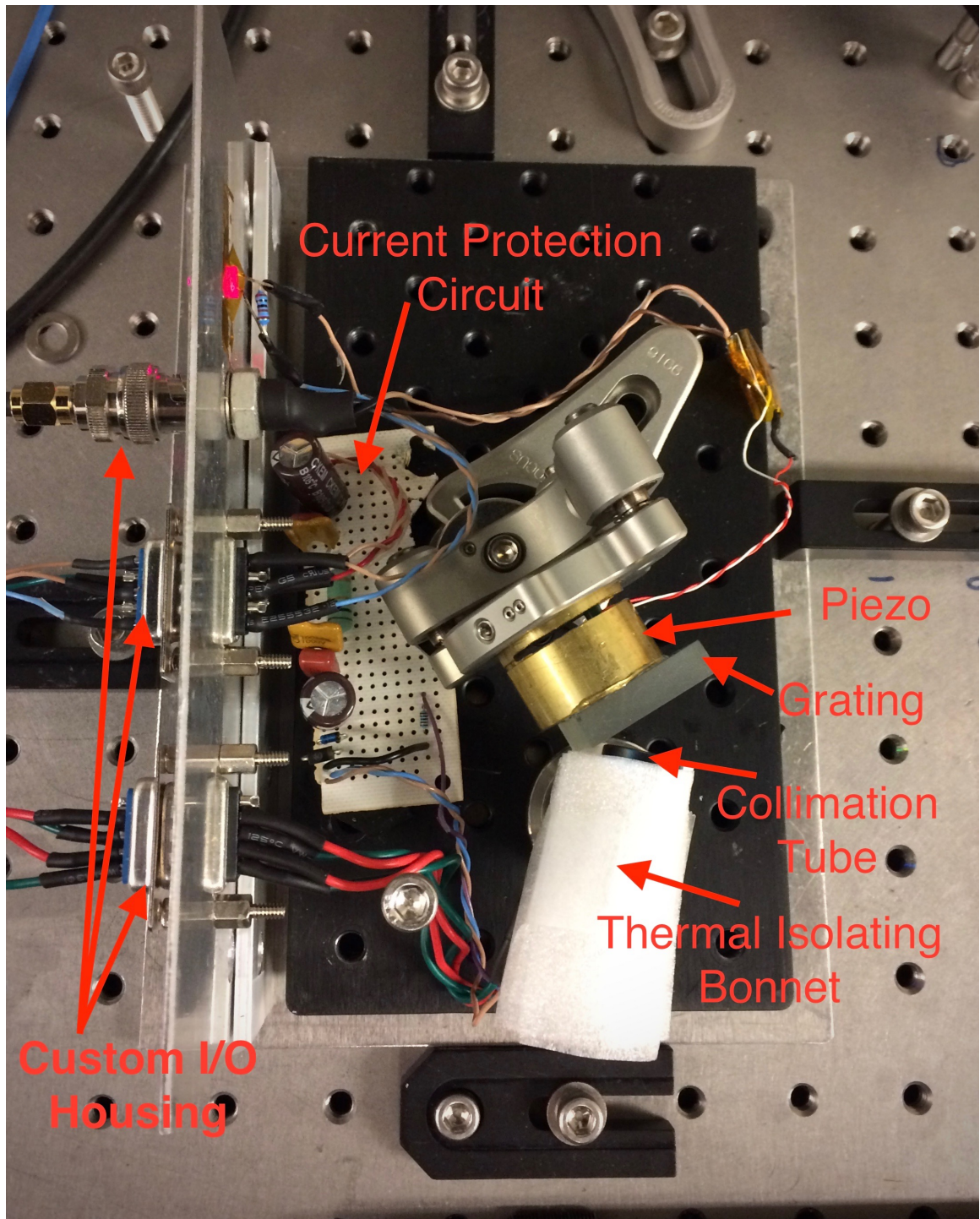


Figure 3.9: Here we can see the internals of the previous set up now rearranged with bonnet over diode and additional control circuitry designed for the current supply. Note that the housing has been removed for this photograph. The I/O ports are arranged, from top to bottom: piezo voltage, current supply for diode, and TEC voltage supply.

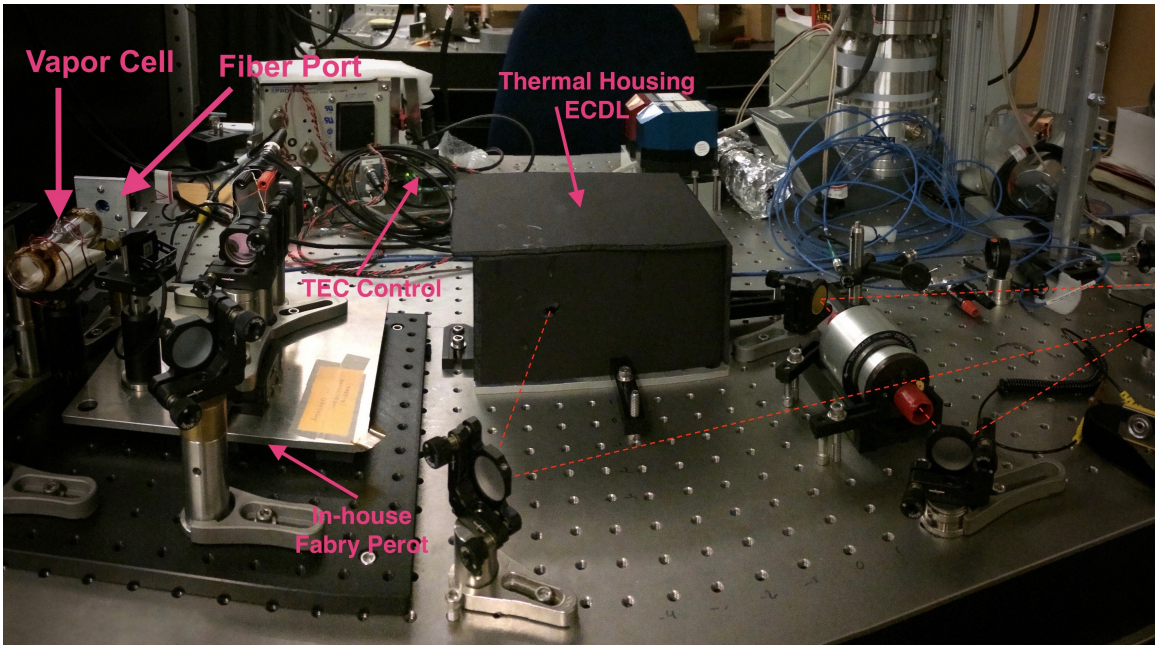


Figure 3.10: ECDL laser and optical setup for diagnostics. Here we can see the externals of the setup which showcases not only the housing used to prevent unnecessary temperature fluctuations but also the general scheme of getting laser light from our ECDL to the vapor cell and Fabry Perot (shown on left in picture).

Chapter 4

Data Acquisition and Achieving Resonance

4.0.1 Getting Near Resonance

The major challenge in this research was achieving resonance by varying the three main parameters: Temperature of the diode, angle of the diffraction grating, and current level for the diode. Making our job more difficult was the relative sensitivity with which our laser would respond to change among any one of the three.

We need to keep track of how each parameters affects the frequency in order to effectively tune the laser. The general relations between parameters and frequency are described in Table 4.1.

Table 4.1: Variance in core parameters (increase or decrease) as they affect laser output frequency (Hz): increase or decrease

	Increase Freq.	Decrease Freq.
TEC (°C)	↓	↑
Diode Current (mA)	↓	↑
Piezo Voltage (grating angle) (V)	↑	↓

These initial findings were used as a starting point for our work getting initial resonance and then further refined in our construction of a feed forward electronics box to help scan over multiple resonance peaks.

4.0.2 Aligning Fiber

After giving the diode power, installing all additional noise reduction devices and achieving feedback with coarse diffraction grating tuning (described in previous sections), we can now move on to understanding how well our laser is functioning. In particular, we would like to be able to control the laser in such a way as to achieve resonance with the rubidium atom at $12816.693 \text{ cm}^{-1}$. This can first be done with a spectrometer to get the coarse tuning out of the way but eventually we need a wavemeter to tell us the exact wavelength of our laser.

However, in order to use a wavemeter, we need to align the output of our laser into an optical fiber. The optical fiber is a thin “wire” made of glass (about the thickness of a single human hair or thinner) which can carry light with little loss in power. To align the fiber coupler, we need to send the output of our laser directly into the core of this fiber. To do this, we use two mirrors and a method of walking opposing mirrors forward and back across one another to align the extremely sensitive fiber coupler.

After an initial signal is obtained, we use a power meter to see how much light is getting through our fiber. If the fiber is well aligned, we expect a high power reading. We adjust until we achieve a maximum of a few mW. Once the fiber is aligned, we simply attach it to the wavemeter and power up the included software to monitor the frequency.

4.0.3 Wavemeter Analysis

A wavemeter is essentially an interferometer where one arm scans back and forth. The separated beams then vary separately in distance with respect to one another. The resulting combination of beams, which is read by a photodetector, varies in accordance with two types of interference: constructive and destructive. The wavemeter can then tell us our output frequency with great precision.

After taking said steps of preparation and tuning, we were able to achieve a frequency of $12816.590 \text{ cm}^{-1}$ (given in wavenumber) which compares well with the resonance of rubidium at $12816.693 \text{ cm}^{-1}$. This is close enough to see resonance of rubidium in a vapor cell — a bright beam of light visible in the infrared via TV camera (see Fig. 4.8).

4.1 Initial Scan Range

4.1.1 Scan Range

Achieving resonance means that our laser is correctly outputting 780 nm light with a significantly narrow linewidth. But one of our goals with the Littrow design was not just to have a laser resonant with rubidium but have a scan range large enough to probe other transitions in rubidium. The rubidium atom has 37 electrons surrounding its nucleus with five orbital shells. These orbital energy levels represent discrete partitions which are known (see Figure 4.1).

Rubidium is an alkali metals which means it only has one electron in the ground state of the 5S shell. It is this electron we will be exciting with our 780 nm laser. Corresponding to Figure 4.1, the $5S_{1/2}$ is excited to the $5P_{3/2}$ and then falls back down to the ground state producing the photons in the 780 nm range (see Figure 4.8).

The four peaks mentioned are those transitions from F_g to F_i as defined in Figure 4.1 (given in order of increasing frequency):

These four transition peaks can be seen in Figure 4.2. When we are scanning, the goal is to see this full spectrum. Our adversaries in achieving this goal are external noise and mode hopping.

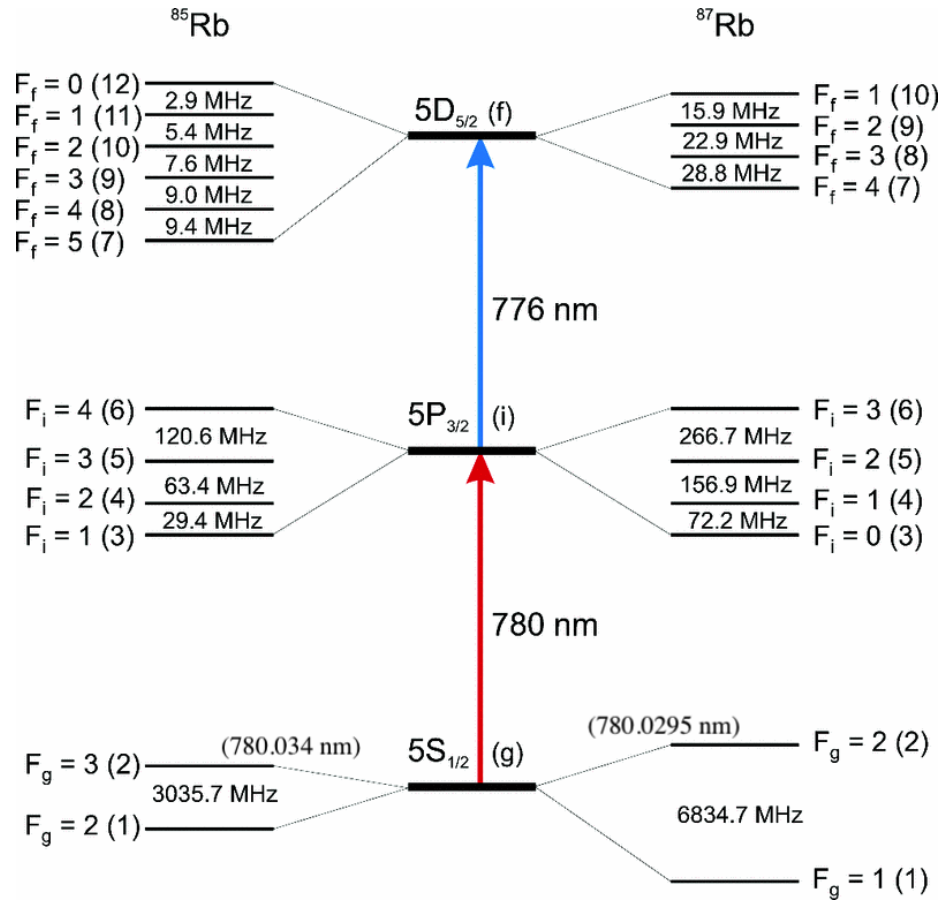


Figure 4.1: Here we can see the levels in Rb. We are only interested in the first of these transitions, those corresponding to 780 nm. Figure adapted from [8]

Table 4.2: Transition peaks given **in order of increasing frequency**. Notice this order matches our Figure 4.1 with the ground state in ^{87}Rb above both ground states in ^{85}Rb and ^{87}Rb 's $F_g = 1$ level is lower than both. The spacing of each, respectively, 3 GHz to 7 GHz can account for this ordering.

	Ground State		Excited State
(Rb 87)	$F_g = 2$	\rightarrow	F_i ($5P_{3/2}$)
(Rb 85)	$F_g = 3$	\rightarrow	F_i ($5P_{3/2}$)
(Rb 85)	$F_g = 2$	\rightarrow	F_i ($5P_{3/2}$)
(Rb 87)	$F_g = 1$	\rightarrow	F_i ($5P_{3/2}$)

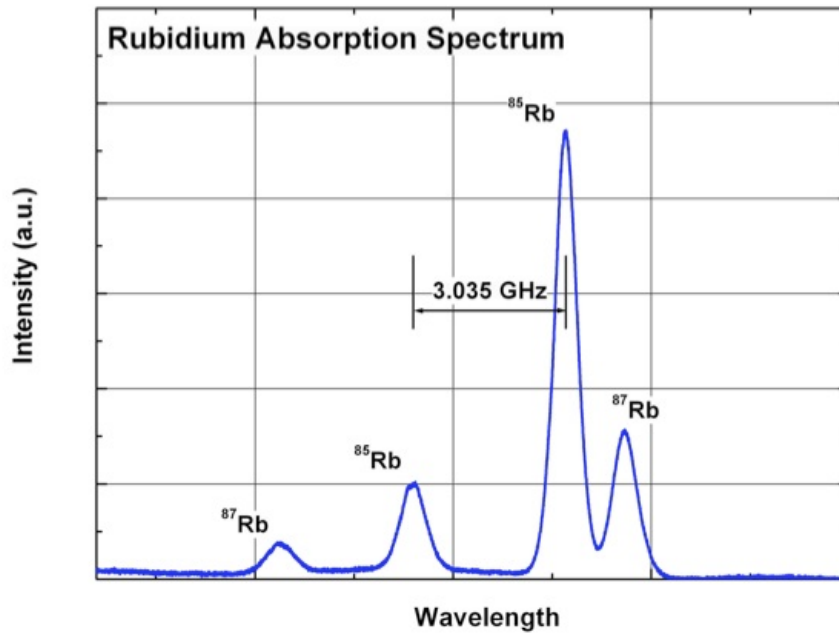


Figure 4.2: Here we see the precise levels of rubidium adopted: Figure adopted from [Photodigm](#)

4.1.2 Manual Scanning

First attempts at scanning through multiple frequencies involved coarsely adjusting both piezo voltage and current, inversely, in accordance with Table 4.1, by hand. This initial method produced very little range but enough to see some evidence of one peak (see Figure 4.3).

In Figure 4.3, we can see what appears to be one peak (with two smaller peaks due to fine level splitting or some other disturbance / back scattering) of the four shown in Figure 4.2. We can see that the Figure 4.3 time increment is on the order of full seconds. This is because our initial method was done solely by hand and, to get the most range, one needed to turn the dials rather slowly. Although it appears to be two peaks, the plot is likely just one peak stretched out, made to look more like

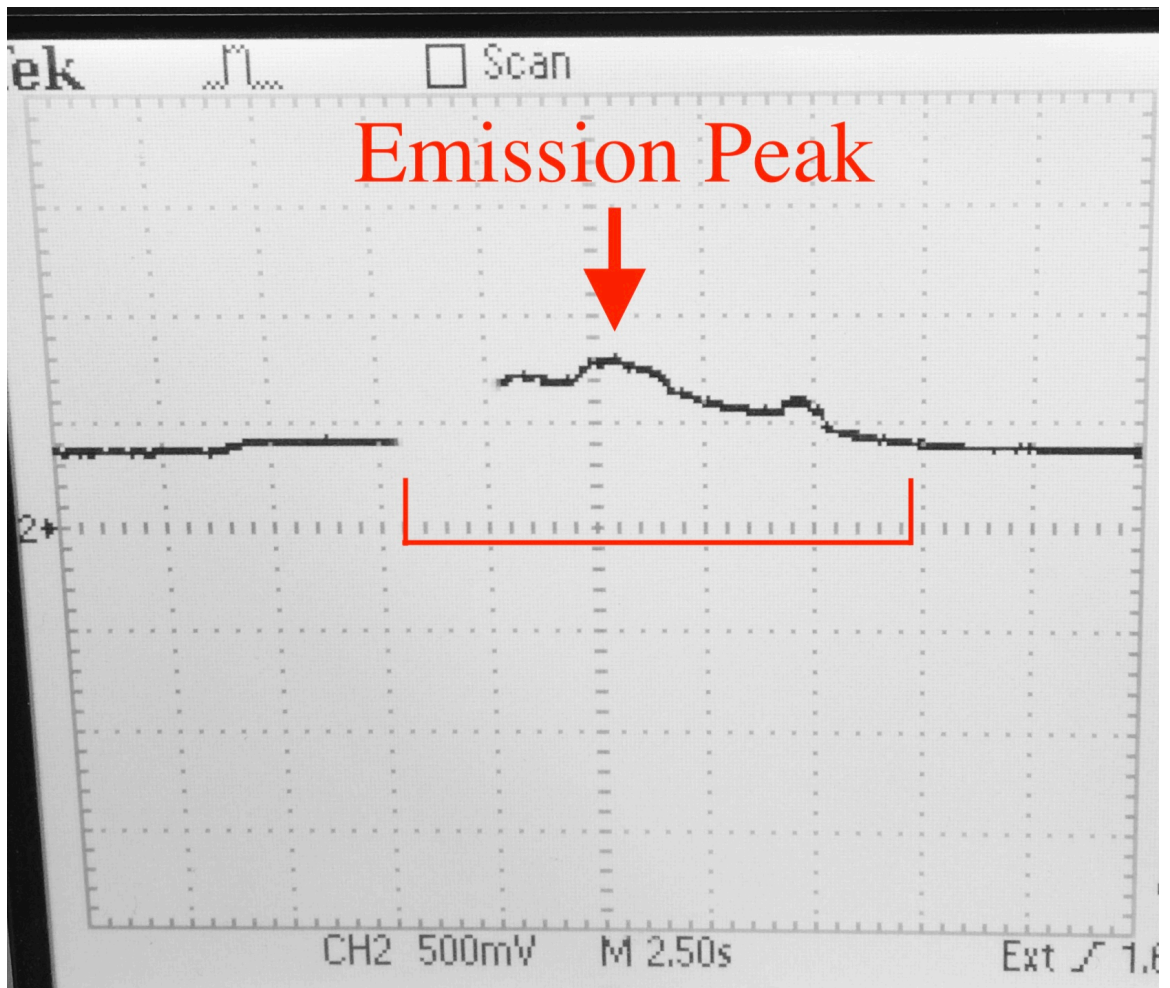


Figure 4.3: This figure shows the emission output of vapor cell while scanning over frequencies of the ECDL constructed. The scanning width is not as wide as we would want but the initial attempt yields promising results. Measured by putting photodiode next to vapor cell for emission detection and changing voltage of piezo and current (thus, laser frequency).

two peaks by this slow rate at which we were scanning.

To improve the scan range, we look to apply the same technique used to acquire the data above in an automated manner.

4.2 Feed-Forward Current / Piezo Scanning Box

To perform such automation, we created a box to control both the current and the piezo voltage simultaneously in reference to a single input voltage provided by a function generator. The ratio of increase between both the piezo and current is controlled by potentiometers. The researcher is then tasked with finding the exact proportions of current increase to piezo decrease and vice versa in which to increase the scan range. As stated previously, the motivation behind an increased scan range is an increased usability of our laser in applications where multiple energy levels of rubidium (and perhaps other energy levels produced with the help of a magnetic field) would need to be reached. Furthermore, the project objective is to produce a well running Littrow ECDL which has a large mode-hop free frequency scan range.

With this in mind, the box was set for construction.

4.2.1 Feed-forward Box Construction

With the relations given in Table 4.1, we know that our box should be constructed to vary current and piezo voltage inversely. Our proposed solution is to use a set of three OP27 operational amplifiers. The diagram shown in Figure 4.4 shows the method we used to achieve the inverse proportionality variation.

The output from the first (inverting) op amp is given by:

$$\text{Output} = V_{input} \left(\frac{-\Omega_{pot}}{200 \text{ k}\Omega} \right) \quad (4.1)$$

The other two op amps take their input voltage from this first op amp and thus both the piezo and current output can be given by, respectively:

$$\text{Piezo Output} = V_{input} \left(\frac{-\Omega_{pot}}{200 \text{ k}\Omega} \right) \left(\frac{-10}{1/6} \right) \quad (4.2)$$

$$\text{Current Output} = V_{input} \left(\frac{-\Omega_{pot}}{200 \text{ k}\Omega} \right) \left(1 + \frac{1\text{k}\Omega}{1\text{k}\Omega} \right) \quad (4.3)$$

We can see the piezo output will be positive while the current will be negative. The piezo requires voltage from 0 - 10 V whereas the current supply takes a bipolar input of -10 V - 10 V.

4.2.2 Voltage Regulators

After initial powering of the box, we observed considerable noise on the output signal, much like that in Figure 4.5. Our first method of attack was to power the device with batteries to eliminate any ground loop problems and to reduce noise in general. Although the noise was reduced, noise was still clearly visible. The noise in the piezo signal is less concerning than noise in the current as the latter is much more sensitive. The equations for the piezo and the current controller, when supplying external voltages are:

For current:

$$I_{LD} = I_{LDSET} + I_{LDMAX} \times U_{MOD}/10V \quad (4.4)$$

$$I_{LD} = 86 \text{ mA} + 200 \text{ mA} \times U_{MOD}/10V \quad (4.5)$$

where 86 mA is chosen because of its initial proximity to resonance and 200 mA is the limit of our model. The former is changed periodically as the main offset for the current portion of our feed forward box.

For piezo voltage:

$$V_{out} = V_{manual} + 15V_{external} \quad (4.6)$$

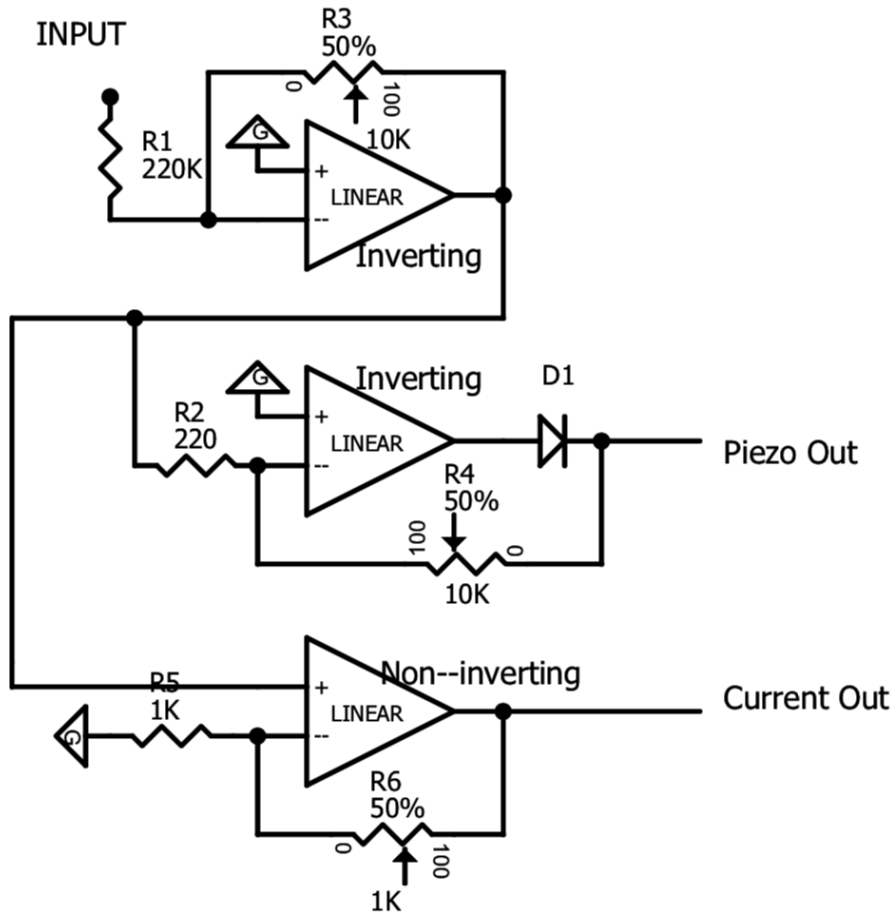


Figure 4.4: We send the input signal into the first inverting amplifier which steps down the signal considerably. Then we amplify for piezo and maintain the low voltage for current as per the specifications of each.

As we can see, the current has a larger factor but, more importantly, the current is inherently more sensitive in changing frequency.

4.2.3 Noise Reduction

Because our initial scanning was still suffering from mode hops, we, yet again, set out to eliminate noise wherever we could find it. A promising culprit was the noisy signal in the current external voltage. The hypothesis was that the spikes could be causing some of the mode hops and, should they be alleviated, the mode hops could be less of an issue.

The solution implemented was to use a simple low pass RC filter with a .4 nF capacitor and 1 k Ω resistor to clean up the high frequency noise. The results can be seen in a before and after comparison in Figures 4.5 and 4.6. Because the sensitivity of current is so much more so than the piezo, and the RC low pass filter we were using only allowed for one input and one output, the current output was chosen and the piezo output was left unaltered.

4.2.4 Increased Scan Range

Our first attempt, show in Figure 4.3 bears just one peak, with poor form, stretched out in the manner described in Section 4.1.2. In Figure 4.7, we can see a clear second peak as well as the long tail making up the valley in Figure 4.2 between the two ^{85}Rb resonant peaks.

We can fit the two peaks with a Gaussian of the following form:

$$f(x) = a1 * e^{-((x-b1)/c1)^2} + a2 * e^{-((x-b2)/c2)^2} + .177 \quad (4.7)$$

with the following fitting constants given with bounds:

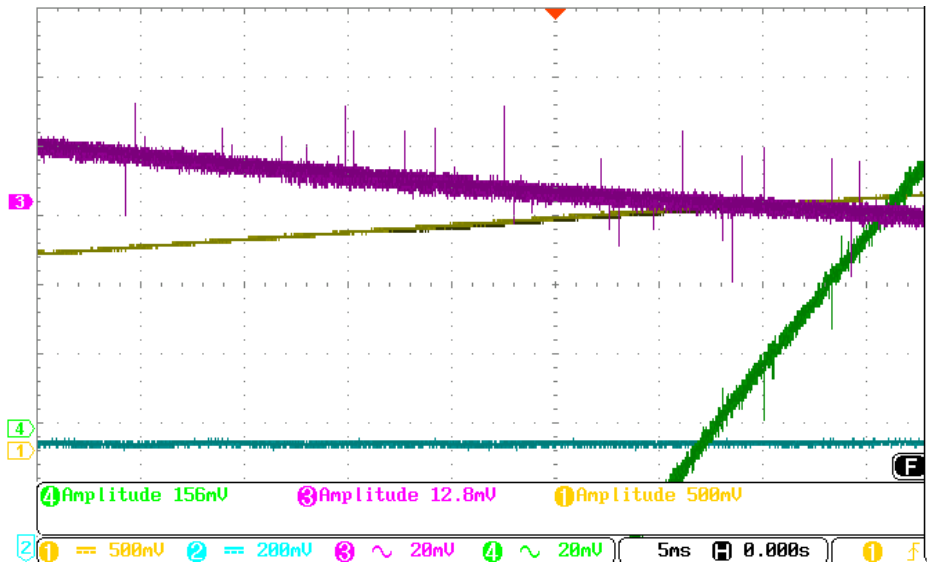


Figure 4.5: Here we see the noise on both the current and piezo signals (enlarged to show detail). Compare with the effects of RC low pass filter in Figure 4.6. Piezo voltage in purple, current in green, input signal in yellow, photodiode in blue.

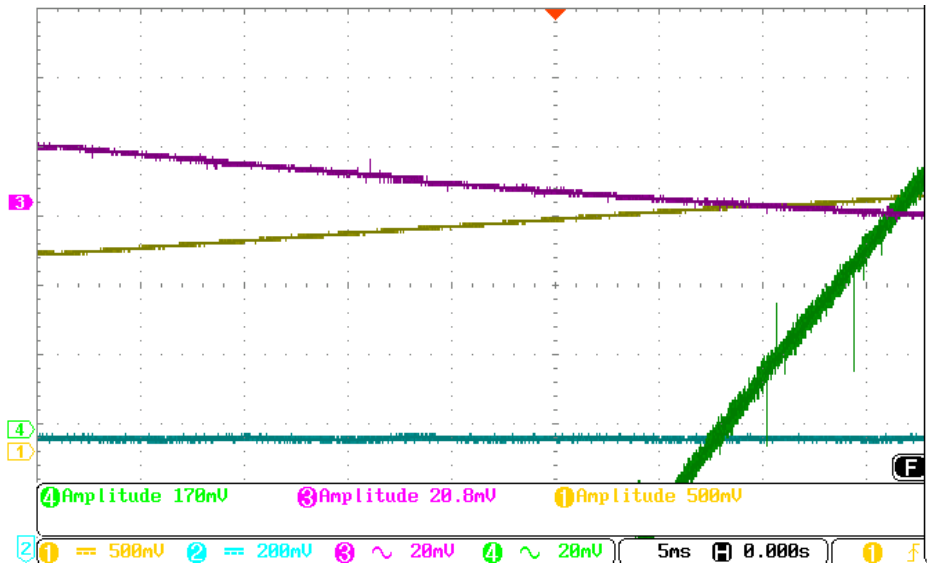


Figure 4.6: Here we see the low pass RC filter working on the purple, current, output, significantly cleaning up the signal when compared to that in Figure 4.5 (enlarged to show detail). Piezo voltage in purple, current in green, input signal in yellow, photodiode in blue.

$$a1 = 0.556(0.5546, 0.5574)$$

$$a2 = 0.2667(0.2655, 0.2678)$$

$$b1 = 7278(7277, 7279)$$

$$b2 = 6210(6208, 6212)$$

$$c1 = 310.6(309.6, 311.6)$$

$$c2 = 499.9(496.6, 503.3)$$

Using the b constants we can get a distance between the peaks, scale it by our 2×10^{-6} factor for seconds and then take the inverse for the frequency. This result can then be compared to the known frequency separation between the two peaks from ^{87}Rb and ^{85}Rb (see Table 4.2). From this fit, shown in Figure 4.7:

$$t = (b1 - b2) * \text{scale factor} = (7278 - 6210) * (2 \times 10^{-6}) = .0021 \text{ s} \quad (4.8)$$

And the frequency difference can be calculated with electron energy levels given in Figure 4.1, second level of ^{87}Rb $5S_{1/2}$ state and second level of ^{85}Rb $5S_{1/2}$ state identified by Figure 4.2:

$$\Delta\nu = \left(\frac{c}{780.0295\text{nm}} - \frac{c}{780.034\text{nm}} \right) \text{GHz} = 2.2188 \text{ GHz} \quad (4.9)$$

Now we know what our scale is, .0021 s corresponds to 2.2188 GHz. With this, we can calculate the total scan range from the beginning of the piezo scan ($x = 5837$) to its maximum ($x = 7929$). As we can see in Figure 4.7, this is a mode-hop free scan.

$$t = (7929 - 5837) * (2 \times 10^{-6}) = .0042 \text{ s} \quad (4.10)$$

And thus the total scan range:

$$\frac{2.2188 \text{ GHz}}{.0021 \text{ s}} \cdot .0042 \text{ s} = 4.4207 \text{ GHz} \quad (4.11)$$

We can see also in Figure 4.7 the issues with mode hopping talked about throughout the paper. The laser jumps from one frequency mode to the resonant mode (the mode resonant with Rb, 780 nm) shown in the graph by the jump in photodiode emission around $x = 5200$. Because we are looking at an emission spectrum from Rb vapor, any jump off of Rb resonance is seen as a sudden drop in emission. The next step is to further reduce noise in the apparatus in order to find what is causing these mode hops and prevent it from occurring.

As we will discuss in greater detail in Chapter 5, this drifting which causes the mode hops is likely due to temperature oscillations from the TEC temperature stabilization system.

4.3 Temperature Drift

Upon completion of the scan box and having successfully collected a large data set, we begin to notice key signs of temperature shift. These shifts are discernible by their signature low frequency noise. In Figure 4.9, we can see that there is clearly low frequency noise (i.e. drifting laser frequency) affecting the output of the laser. This finding motivates further testing into the temperature stability of the temperature controller and the final temperature reading of the Peltier TEC.

4.3.1 IR Camera

For preliminary testing, we use a camera, sensitive in the infrared to see what sort of temperature gradients we are dealing with and to see whether or not the diode is being subject to temperature oscillations. The IR camera is limited in resolution and accuracy but we can clearly see, in Figure 4.10, that there is a potential danger

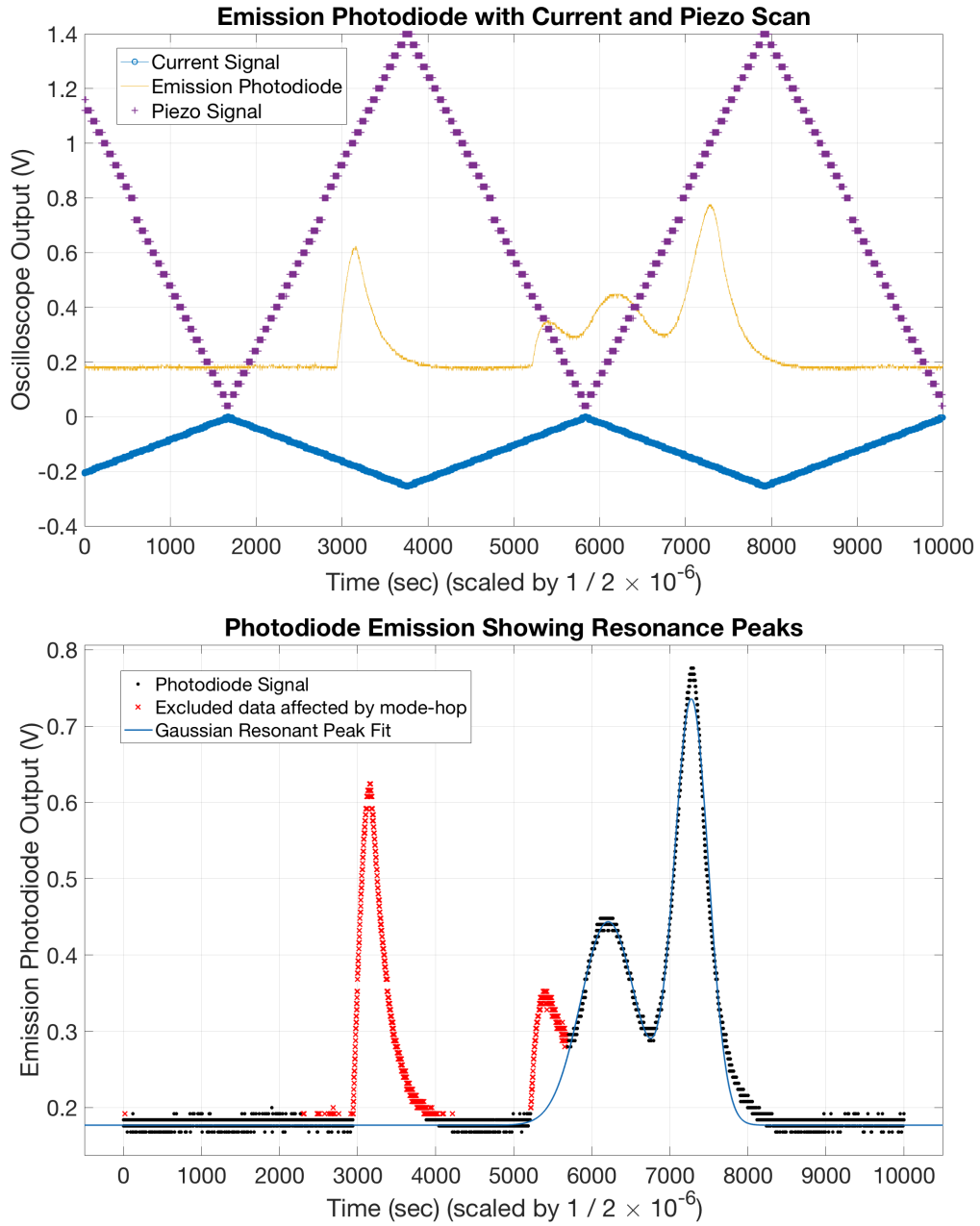


Figure 4.7: The emission photodiode output included with the piezo and current scan (TOP) and the isolated emission scan fitted with two Gaussian peaks (BOTTOM). The fit gives us an exact location for the peaks and thus another way to read the frequency difference in the scan.

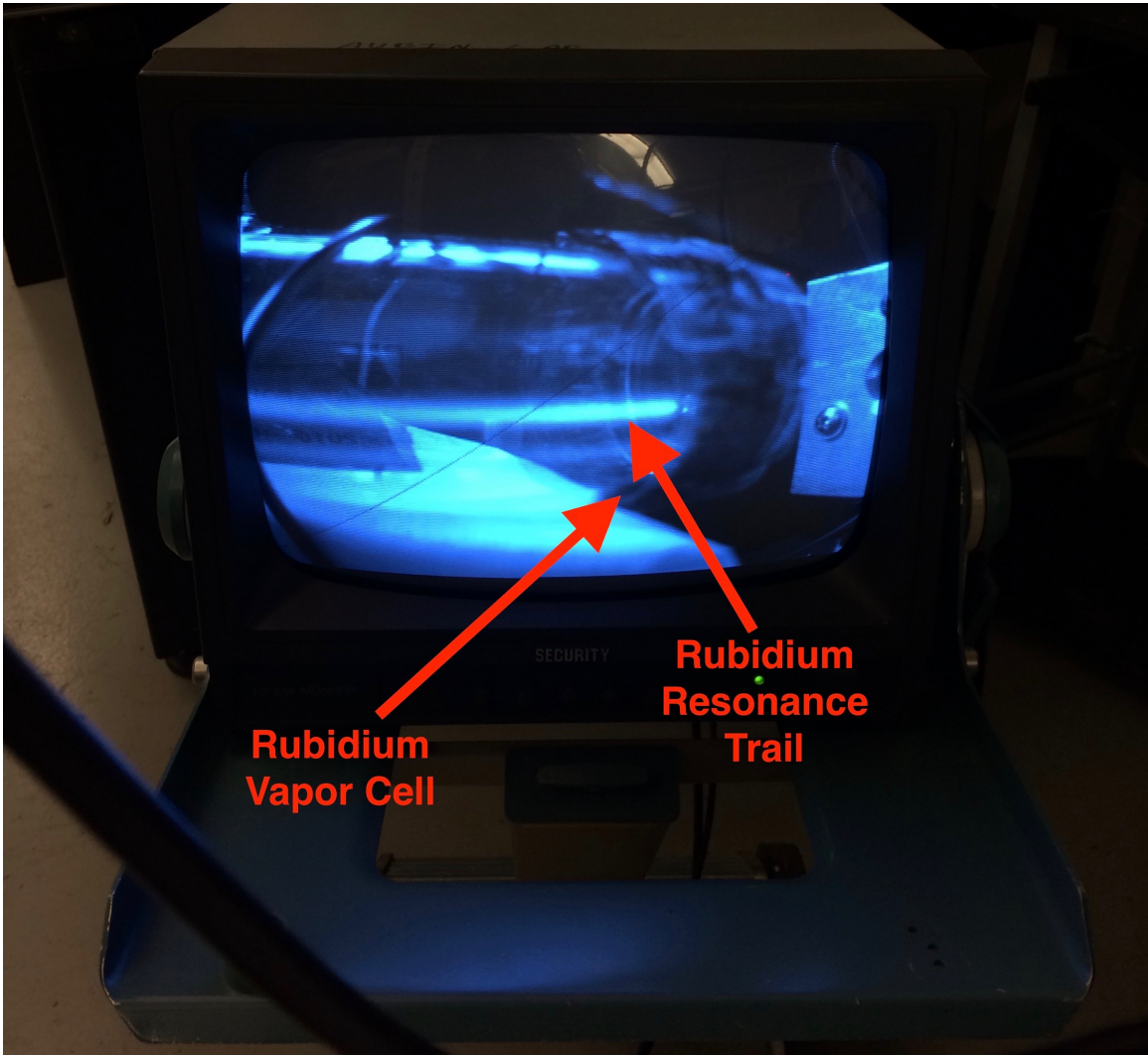


Figure 4.8: Here we can see the vapor cell at resonance. The beam shown means our laser is correctly calibrated for rubidium transitions. What is left remaining is creating a more stable resonance.

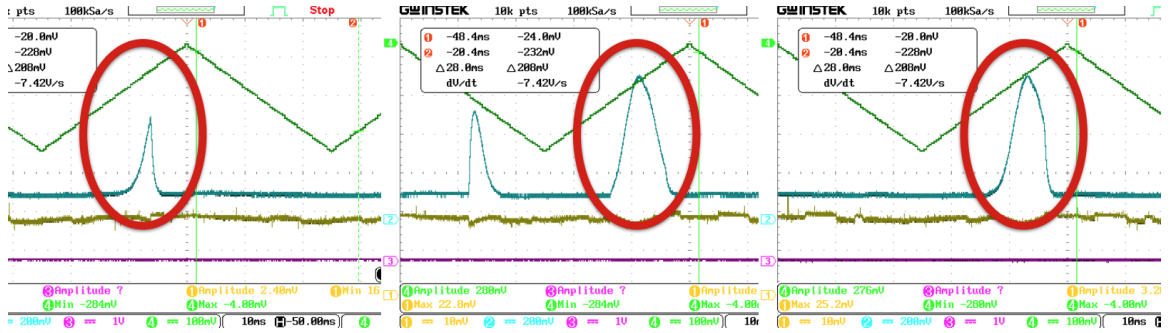


Figure 4.9: We can see here three oscilloscope screen captures. The images were captured on the order of 5 seconds of separation. We can see clearly a very gradual change in lasing frequency as shown by the changing emission photodiode output (in blue, peak). Here we can also see mode hops.

in the form of a very high temperature gradient and also evidence of temperature oscillations in the coarse measurements of the infrared camera.

4.3.2 Thermistor Data Acquisition

After seeing evidence of temperature drift both in the oscilloscope output and the infrared camera, we decide to get more data through the installation of a D9.7a Thermometrics thermistor onto the Peltier TEC.

By combining the resistance data with the known temperature equation for the our NTC thermistor, we can produce a temperature oscillation graph (see Figure 4.11). Such oscillations are more than enough to adjust the output frequency of our laser. Such unpredictable parameter changes are likely the cause of the laser's lengthy calibration times thus far. Having stable, reliable parameters will make finding resonance and tuning the resulting laser output much more straight forward and less likely to drift and mode hop.

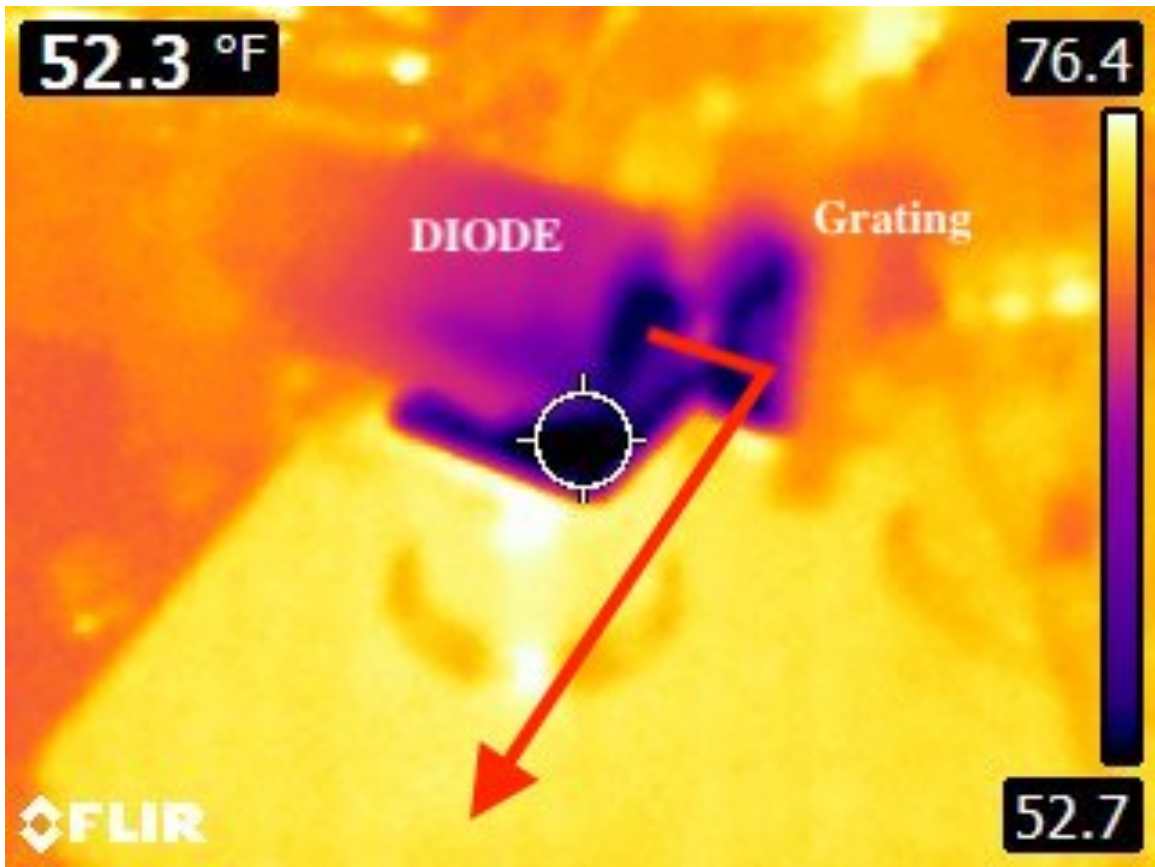


Figure 4.10: We can see here a shot in the infrared of the laser diode and the grating (left to right). The Peltier is the cooling element. Setting the camera as steady as possible and reading the output, we note a coarse temperature range of 1 degree celsius and are motivated to look into the problem further.

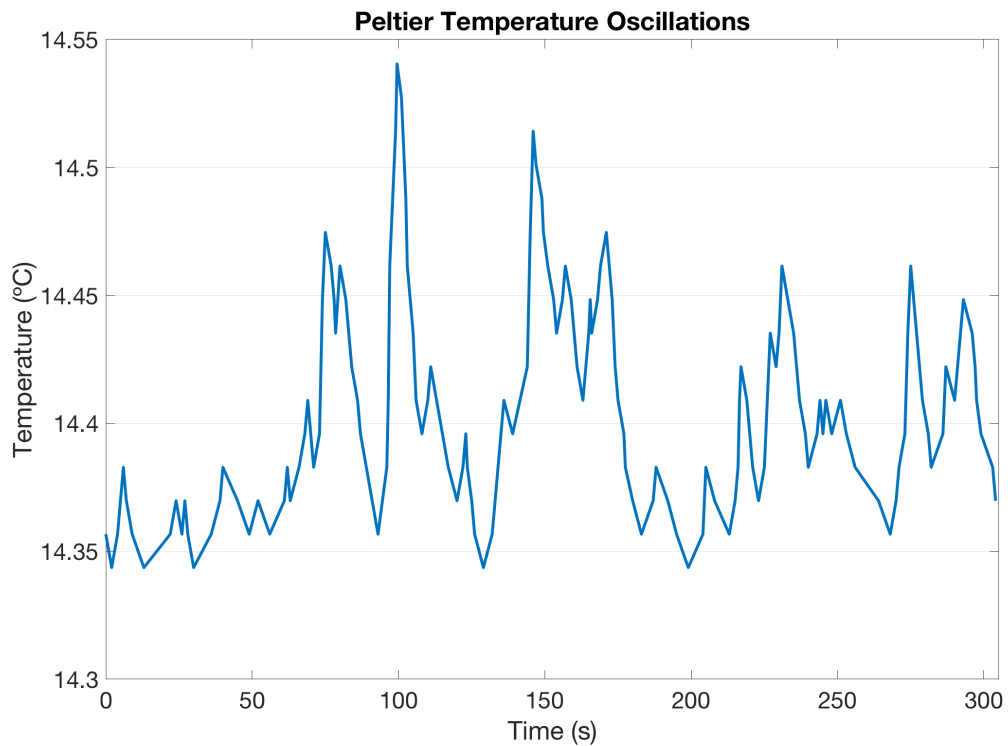


Figure 4.11: Temperature change of the Peltier TEC as a function of time. We can see that the max change in temperature is $.2\text{ }^{\circ}\text{C}$ which corresponds to a maximum cavity length change on the order of micrometers which can significantly change the output frequency (nanometer scale) of our laser. This is in contrast to the LED readout of the TEC.

Chapter 5

Results and Conclusions

5.1 Results

This thesis shows that an in-house ECDL using the Littrow design is feasible provided one takes into account possible sources of noise – specifically thermal and mechanical.

After thoroughly isolating our ECDL mechanically — through sorbothane and aluminum vibrational damping, I/O ports removed from the laser base plate, and flexible wires — and thermal isolation — through housing of the entire setup and inner housing of the diode (see Figure 3.9 and Figure 3.10) — the ECDL was functional but still exhibited significant frequency drifts. This drifting was on a very long time scale, with a period > 30 sec. The likely culprit in this scenario is temperature which oscillates on exactly these sorts of times scales.

In order to test this hypothesis, we attached a thermistor to the Peltier connected to the TEC. The Peltier showed that the temperature was indeed oscillating, sometimes by as much as $.2^{\circ}\text{C}$. This is more than enough to cause a significant change in the gain medium and drift the frequency of the ECDL's output showing up as mode hops in Figure 4.7.

5.2 Outlook

In the very near future, one should look to solve the temperature oscillation issue and extend the scanability of the laser. A possible remedy is simply to replace the temperature controller with one that is more precise. If swapping controllers does not solve the temperature oscillations, another solution, keeping the core of the Littrow design, would be to move the system itself onto a thermally controlled base plate thus preventing any severe cavity changes.

Once the scanability is increased and greater stability is achieved we can look to apply the laser within the AMO laboratory. Specific applications could vary from observing transitions at high magnetic field to photo-associating molecules[2].

5.3 Conclusion

In this thesis, we have achieved resonance in a rubidium vapor cell and saw the first signs of its atomic fine structure all using a Littrow design ECDL constructed from the ground up. We note that thermal oscillations from the Peltier TEC may explain mode hops within frequency scans (Figure 4.7).

By implementing our feed-forward scanning box, we have increased our scan range to 4.4 GHz. Furthermore, the constructed feed forward scanning box allows us to achieve resonance with much more automation than previously was possible, alleviating what is perhaps the most time consuming aspect of ECDL work, calibration.

Bibliography

- [1] M. K. Ivory, A. R. Ziltz, C. T. Fancher, A. J. Pyle, A. Sensharma, B. Chase, J. P. Field, D. J. A. Garcia, and S. Aubin, Atom chip apparatus for experiments with ultracold rubidium and potassium gases, *Rev. Sci. Instrum.* **85**, 043102 (2014).
- [2] B. Chase, Developing a dipole trap laser for the purpose of cold and ultra-cold molecule production, Senior Thesis (College of William and Mary) (2012).
- [3] C. J. Hawthorn, K. P. Weber and R. E. Scholten, Littrow configuration tunable external cavity diode laser with fixed direction output beam, *Rev. Sci. Instrum.* **72**, 4477 (2001).
- [4] M. Scholl, Interference filter stabilized external cavity diode laser, Technical Report (University of Toronto) (2010).
- [5] D. J. Thompson and R. E. Scholten, Narrow linewidth tunable external cavity diode laser using wide bandwidth filter, *Rev. Sci. Instrum.* **83**, 023107 (2012).
- [6] Joseph H. Thywissen and Seth Aubin, personal communication, June 20, 2017.
- [7] D. W. Preston, Doppler-free saturated absorption: Laser spectroscopy, *Am. J. Phys.* **64**, (1996)

- [8] N. Vujcic, T. Ban, G Kregar, D. Aumiler and G. Pichler, Velocity-selective double resonance in Doppler-broadened rubidium vapor, *Physical Review A*. **87**, (2013)